Additive Manufacturing 39 (2021) 101840

Contents lists available at ScienceDirect

Additive Manufacturing

journal homepage: www.elsevier.com/locate/addma

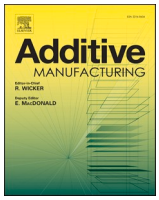

Research Paper

Reusable support for additive manufacturing

Yang Xu [a], Ziqi Wang [b], Siyu Gong [a], Yong Chen [a,*]

[a] Daniel J. Epstein Department of Industrial and Systems Engineering, University of Southern California, Los Angeles 90089, CA, USA
[b] School of Computer and Communication Sciences, EPFL, CH-1015 Lausanne, Switzerland

ARTICLE INFO

Keywords:
Additive manufacturing
Material extrusion
Reusable support
Programmable platform
Layout optimization

ABSTRACT

Additive manufacturing (AM) processes such as material extrusion and vat photopolymerization all require supports to print parts with overhang features. These additional supports using the same or different materials are a waste of materials since they need to be removed after the three-dimensional (3D) printing process and cannot be reused. The printing of supports is also time-consuming for the nozzle-based material extrusion processes. A new type of reusable support has been developed to address the support-related challenges in AM. The main idea is to use a set of dynamically controlled metal pins as a programmable building platform. In the layer fabrication, the metal pins will move up one-layer thickness after the printing of each layer. Also, each metal pin will automatically stop at a specified height that is determined by a combination of metal tubes, magnetic discs, and magnetic rings. Additional supports can be 3D-printed on the top surface of the metal pins, while the amount of the supports is dramatically reduced. After the printing process, the metal rods can be separated from the part and reset for the next printing job. A prototype system has been constructed to demonstrate the reusable support principle. The layout optimization and toolpath generation algorithms for the reusable support are also presented. The experimental results of several test cases show an average of nearly 40% saving on the printing time and material with increased reliability and robustness. The reusable support provides a support generation strategy that could be beneficial to other AM processes such as stereolithography and selective laser melting.

1. Introduction

Additive manufacturing (AM) technology uses a layer-based fabrication process. The printing material can only be deposited on the top of an existing surface. The limitation is problematic for three-dimensional (3D) complex parts with overhang structures since such overhangs cannot be printed without supports that are immediately beneath them. The AM processes, such as fused filament fabrication (FFF) and stereolithography apparatus (SLA), solve this problem by creating additional supporting structures for the overhangs [1]. The 3D-printed supports could use the same or different materials, such as water-soluble material [2] and even ice [3]. The supports will then be discarded after the fabrication process finishes. Therefore, the support generation is a critical issue for AM technology since the 3D-printed supports leads to longer fabrication time, more material waste, and extra post-processing time [4].

1.1. Related works

Most existing solutions to reduce the required supports are geometry-based approaches. These methods can be divided into three categories. For a given computer-aided design (CAD) model, one approach is to select a suitable orientation of the CAD model to cut down the support volume [5]. Besides support volume, several other aspects such as surface quality, building time, part accuracy, or contact area were considered in these studies [6–12]. The second approach is to reduce the 3D-printed supports by modifying the CAD model itself. Mirzendehdel and Suresh [13] proposed a topology optimization method based on the constraint of support volume. Another straightforward way is to divide 3D models into multiple small pieces to reduce the required support and the printing time for a large model that may exceed the size of the printing tray [14]. Vanek et al. [15] converted the input 3D model into a shell before cutting it into multiple segments. Then the small pieces are tightly packed to minimize the support material consumption and the bounding box volume. Hu et al. [16] decomposed the 3D models into a set of pyramidal segments to remove additional supports since

* Corresponding author.
E-mail address: yongchen@usc.edu (Y. Chen).

https://doi.org/10.1016/j.addma.2021.101840
Received 3 September 2020; Received in revised form 6 December 2020; Accepted 5 January 2021
Available online 12 January 2021

pyramidal shapes have no overhang features. Jiang et al. [17] proposed a strategy to optimize the layout of multiple parts, including position and orientation of each part with the aim of reducing support consumption. However, these two approaches require either changing the building orientation or the manual assembly of multiple small pieces, which could be problematic for many applications. In our work, we assume that the input CAD model will not be modified; also, a build orientation for the model has been selected by the user and will not be changed.

The last approach is to reduce 3D-printed support by developing better support structure and optimizing the layout of the support [18,19]. The most common support shape is the vertical solid-wall-like structure that connects the surface facets whose tilting angle is large than a threshold value (e.g., 45 degrees used in the commercial software systems such as MakerBot and Simplify3D). This type of support ensures reliability at the expense of increased printing time and material. Instead of vertical wall-like support, Huang et al. [20] presented a sloping wall-like support structure, in which the size of the middle portion of the vertical wall-like supports is reduced. Similarly, Strano et al. adopted density-changeable cellular structure to reduce the support volume [21]. Unlike classical external supports that touch the building platform, Cacace et al. proposed an algorithm that converts all the external supports to internal ones with both ends of the supports connecting to the part itself [22]. Consequently, the support volume and printing time are reduced. However, the method only works for chamfer features. For cantilever features, the material consumption of this method is larger than that of the classical external support.

Instead of generating support for the whole overhang area, Meshmixer from *Autodesk* [23] and Vanek et al. [24] proposed a new kind of support that only touch the part at sparse points within the overhang area. Similar to the natural tree, these supports will converge from the supporting points progressively and form a set of brunches. Finally, the vertical or non-vertical trunk-like pillars are generated to support the branch-like supports. In this way, much less support material will be used. However, the printing process may be unstable or even fail in some cases, mainly because the printing of slanted pillars is less reliable than the printing of vertical pillars due to the smaller bonding areas between layers and the uneven warping during the cooling process [25]. Besides, the weight of the branch-like pillars and the torque generated by the printhead tends to bend the structure, which may cause deformation and lead to failure eventually. Dumas et al. [25] presented a scaffolding-like support structure based on bridging effect for FFF. Different from the long and slanted tree-like supports, wide horizontal bridges with short slanted pillars were used to connect the points to be supported. Then sturdy vertical pillars were used to support the bridges, which improved the printing reliability at the expense of slightly increased material usage and printing time. Recently, Jiang et al. further studied the bridge effect [26] and proposed two support generation methods based on this effect to reduce external and internal support volume [27,28].

In addition, Barnett and Gosselin [29] proposed two support strategies for FFF by using materials such as foam and gel to lower the material cost and to facilitate easy support removal. The first strategy is called the shell technique. A strong material was first extruded to form an enclosed shell, and a weak material (e.g., shaving foam) was then deposited to fill the space between the shell and the part. The shell technique is robust and compatible with any part geometry; however, it is time-consuming due to the large support volume. The second strategy was called film technique. That is, a weak material works as a thin film between the part and the rigid support to facilitate the support removal. However, whether this technique could work depends on part geometry. The surface quality of the fabricated part is also not as good as the traditional approach.

Unlike the aforementioned strategies, Shen et al. [30] presented a flexible support platform for support reduction, similar to the work presented in this paper. Inspired by a digital clay [31,32] and a 3D shape display (inFORM) [33,34], each metal pin in the flexible support platform is actuated by a dedicated linear stepper motor with a control chip and a motor driver, so each pin can be moved up/down during the fabrication process [30]. However, the stepper motor size restricts the minimum pin size. More importantly, a higher resolution or a larger platform size would require more metal pins, which leads to the same number of additional stepper motors, drivers and controllers. Besides soaring cost, the complexity and reliability of controlling hundreds or thousands of stepper motors is challenging. The unloading of the flexible platform may damage fragile features of digital models. All these issues will be addressed in this paper.

1.2. Our approach and contributions

Regardless of how the supporting structure and layout are optimized, the 3D-printed supports are a waste of material since they must be removed and cannot be reused after the printing process. Also, for the material extrusion processes, the printing speed is largely slowed down by the extra time required to print these supports. In this paper, a new type of reusable support structure composed of a set of flexible pin array has been developed for AM processes, such as FFF. In our reusable support design, only one motorized linear stage is used. The use of a single linear stage to control the movement of a large number of metal pins is dramatically different from the reusable support design presented in [30]. One test case based on the newly developed reusable support is shown in Fig. 1, and the printing results compared with the traditional method side-by-side are shown in Fig. 1a–c. The toolpath of a random layer of the printing job (the 178th layer indicated by the white dash line) is shown in Figs. 1d and e. The toolpath using the reusable support is much shorter than that of the traditional method (11 mm vs. 5 mm). Hence both printing time and material waste are significantly reduced. Also, the reusable support significantly enhances fabrication reliability, especially for tall features. For example, the 3D-printed support marked in Fig. 1b in a rectangle was bent during the printing process. When the overhang feature is tall, the force added by the moving nozzle leads to a large torque to the support, which may lead to printing errors or even failure. In comparison, the 3D-printed support based on the planned reusable support was significantly shorter (Fig. 1a). The metal pins used in the bottom portion are three orders of magnitude more rigid than the 3D-printed support structure. After the printing process, the metal pins can be easily removed from the built parts without damaging fragile features since each metal pin can be removed from the built parts using a magnetic ring (refer to a video in the supplementary).

Supplementary material related to this article can be found online at doi:10.1016/j.addma.2021.101840.

Our reusable support method is general for any given 3D objects. It can also be combined with different support structures and materials mentioned in the previous research. One limitation is it can only reduce the support for the features that are accessible to the building platform. For the overhang features that cannot be reached from the building platform, the same support structures can be used. Compared with the reusable support in [30], a limitation of our method is the height of each pin is determined by a set of pre-fabricated tubes with some standard lengths. To address the related support efficiency issue, a prototype software system has been developed for the reusable support, in which the automatic layout optimization of input CAD models and the toolpath planning of the 3D-printed supports on the movable support platform have been addressed. Inspired by our work, we believe more reusable support methods, designs, and algorithms will be developed for AM technology in the future.

The rest of the paper is organized as follows: the hardware design of the reusable support is presented in Section 2. The printing process, based on the developed reusable support, is also described in the section. The software development based on the reusable support is presented in Section 3, including a layout optimization algorithm for input CAD models and the toolpath generation of the 3D-printed support on metal pins. The experimental results of several test cases are presented in

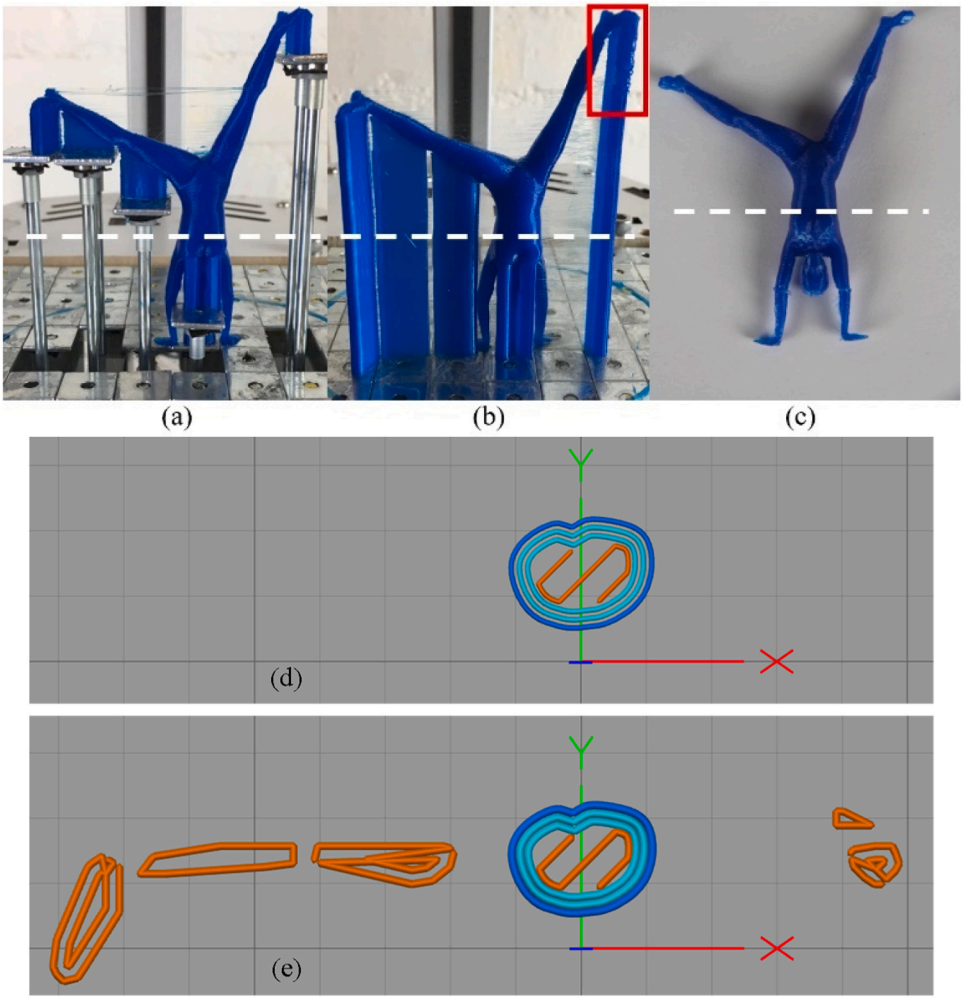

Fig. 1. A Gymnast test case. (a) The printing result with reusable support. (b) The printing result without reusable support. (c) The fabricated object after removing the support. (d) The tool path of the 178th layer in (a) – marked by the white dash line (printing time: 19 s; extrusion length: 5 mm). (e) The tool path of the 178th layer in (b) – marked by the white dash line (printing time: 37 s; extrusion length: 11 mm).

Section 4 with the result analysis. Finally, conclusions are drawn with future work in Section 5.

2. Reusable support design and printing process

The reusable support can have several possible configurations based on different 3D printing processes and their requirements on support. In this section, a design configuration for the FFF process is presented. Other variations of the reusable support mechanism can be made based on a similar design principle while considering different support requirements, e.g., selective laser melting (SLM) will require larger attaching force and additional heat transfer path.

2.1. Basic principle

The schematic diagram of the reusable support is shown in Fig. 2. The apparatus is composed of a set of metal pins and a three-layer-sheet structure. Both the first-layer and second-layer sheets are fixed to the frame, while the third-layer sheet is connected to a motorized linear stage controlled by the motion controller of the FFF 3D printer (Fig. 3). During the layer fabrication, the third-layer metal sheet will be moved up the same layer thickness as the extrusion head after the printing of each layer. Initially, the metal pins whose top surfaces serve as the movable printing platform sit on the first-layer sheet. A metal pin will be lifted with the third-layer sheet if a pre-fabricated hollow tube with a magnetic disc on the bottom and a magnetic ring on the top is inserted from the base into the metal rod (Figs. 2 and 3). Since both the second-layer and the third-layer sheets are magnetic metals (e.g., steel), the magnetic disc and the magnetic ring on both sides of the metal tube will fix the rod either to the third-layer sheet or the second-layer sheet,

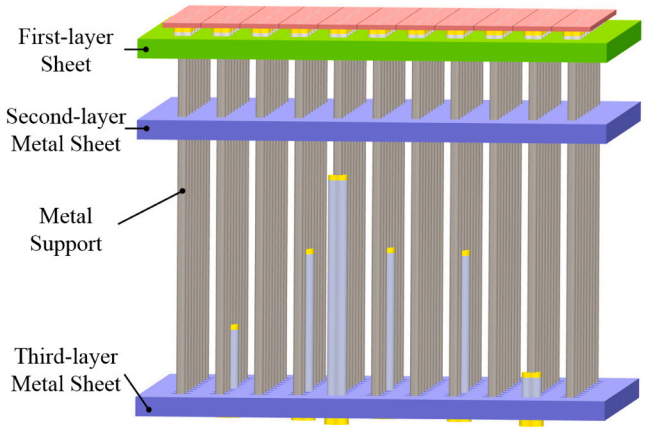

Fig. 2. The schematic diagram of the reusable support apparatus with the 3-layer sheet structure design.

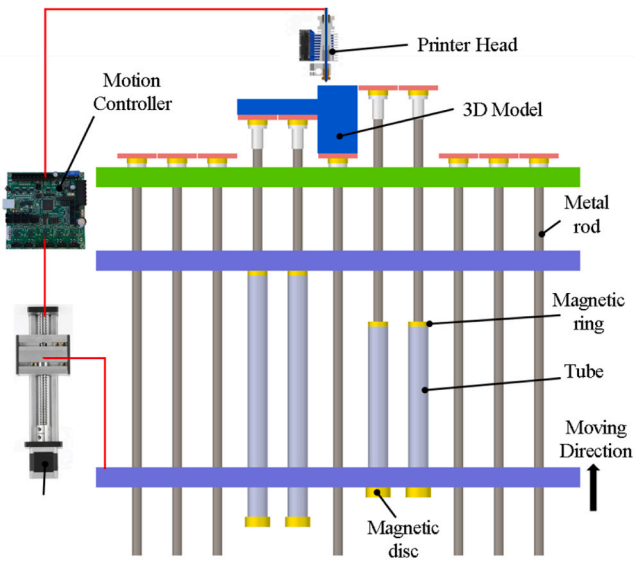

Fig. 3. The schematic diagram of a FFF printer based on the reusable support.

respectively. Consequently, the metal pin will be lifted layer by layer and finally fixed at a certain height during the layer-based printing process.

If no tube is inserted into the rod of a metal pin, the pin structure will remain on the top surface of the first-layer sheet without any movement when the third-layer sheet continuously moves up. All the metal pins with inserted tubes will move up the same distance as the third-layer sheet. Further, a metal pin will stop when the top magnetic ring of the inserted tube reaches the second-layer sheet. Afterward, the bottom magnetic disc of the inserted tube will detach from the third-layer sheet when the third-layer sheet continuously moves up (Fig. 3). The metal pin will remain at the same height since the top magnetic ring attaches to the second-layer sheet and fixes the metal rod with the inserted tube and the bottom magnetic disc. Consequently, the metal pin will provide a movable building platform for the printer head to deposit material on during the remaining fabrication process.

In our reusable support design, a single motorized linear stage can move hundreds of metal pins up and down with synchronized motion; at the same time, each metal pin can be stopped at the desired height using a pre-selected metal tube. Accordingly, a set of metal pins, a 3-layer-sheet structure, and an extra motorized linear stage are required as the additional components in a FFF 3D printer integrated with the reusable support (Fig. 3). All the components required in our design are inexpensive. Also, if selected with standard sizes, most of the components (e.g., rod, washer, magnetic ring, magnetic disc, etc.) can be purchased off-the-shelf. In the remainder of the section, the structure design and some main components are explained in detail.

2.2. Pin-like support and the first-layer sheet

The first-layer sheet is a fixed plate that holds all the metal pins at their original places that define the printing platform (Fig. 4b). During the 3D printing process, the pin-like reusable support will be lifted to serve as the movable building platform. Fig. 4a shows the detailed design of the metal pin structure. Each metal pin is composed of a metal rod, a square metal washer, a magnetic ring, and a sleeve. The sleeve fixes the magnetic ring at the top of the metal rod, and the metal washer adheres to the magnetic ring due to the magnetic force. All the metal pins sit on the fixed first-layer sheet (Fig. 4b). In our prototype system, we designed 11 × 9 pins. Each metal pin will provide a programmable anchor surface for 3D-printed parts and supports. The added magnetic ring beneath the washer is for the 3D-printed parts and supports to be easily taken off after the fabrication process (refer to the supplementary video). After peeling off the attached metal washers, the built object can be easily separated from the reusable supports. Afterward, the metal washers can be removed from the 3D-printed parts and supports and put back on the top of the metal pins. The reusable support is ready for another printing job.

2.3. Inserted tubes and the second- and third-layer sheets

The stop position of each metal rod is determined by the inserted metal tube that has a magnetic ring on both its top and bottom sides (see Fig. 3). A set of pre-fabricated tubes with standard lengths (e.g., 10 mm, 50 mm, 100 mm, etc.) can be provided with the FFF printer (similar to a set of Gauge blocks with standard sizes). Since all the components of the metal tubes are inexpensive, a large number of tubes with magnetic rings at various lengths can be fabricated and provided to the user. In addition, tubes with different lengths can easily be combined with the aid of magnetic rings to get much more combined lengths. For the input CAD models of a printing job, a software system will plan the CAD model layout on the platform (refer to Section 4) and tell the user which tube (or combined tubes) to select from the set and be inserted onto which metal pin. The tubes can also be picked and inserted by a robot or a tube-inserting system in the future, similar to the automatic tool changer in a computerized numerical control (CNC) machine.

A selected tube can be inserted onto a metal pin from the bottom side of the third-layer sheet until the bottom magnetic disc firmly attaches to the metal sheet. Afterward, the pin will be moved up with the third-layer

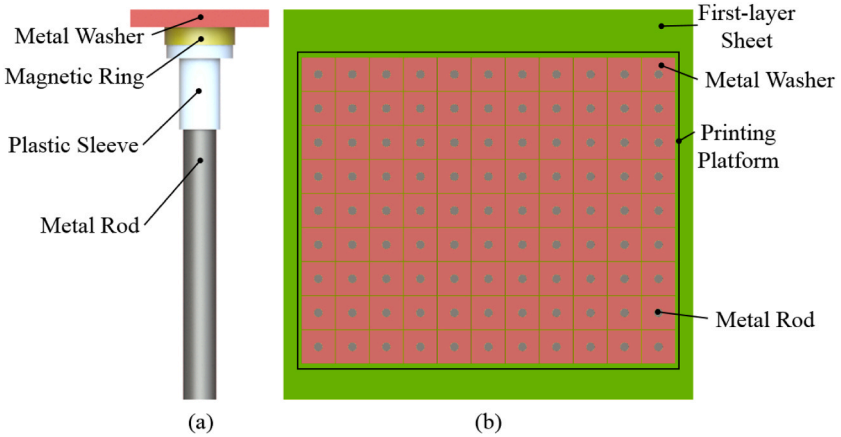

Fig. 4. The detailed structure of a metal pin structure and the first-layer sheet. (a) The design of the metal pin structure; and (b) the printing platform using a set of reusable metal pins (a total of 11 × 9 metal pins are used in the design).

sheet. When the top magnetic ring of the tube touches the second-layer metal sheet, the metal pin will no longer be able to move up due to the fixed length of the tube. After the separation of the bottom magnetic disc from the third-layer sheet, the metal rod will be fixed to the second-layer sheet. During the remaining process, the metal rod will maintain at the same height, although the third-layer sheet will continue moving up. After the printing job finishes, the lifted metal pins can be automatically pulled down to its original position when the third-layer sheet moves down. This can be easily achieved by selecting the bottom magnetic disc with a larger magnetic force than the top magnetic ring.

2.4. Printing process based on the reusable support

In summary, the revised FFF process using the reusable support is given as follows.

(1) Before the printing process, the tubes with magnetic rings at the top and magnetic discs at the bottom will be added to the metal pins where the pins will be raised up during the printing process (Fig. 5a). Where to add the tubes will be determined by a software system.
(2) When the printing job starts, the metal pins with the inserted metal tubes will move up by one-layer thickness after the printing of a layer (Fig. 5b).
(3) The inserted tube will stop the metal pin's movement once the tube touches the second-layer sheet. The metal pin will be attached to the second-layer sheet afterward (Figs. 5c and d).
(4) For a metal pin at a certain height, 3D-printed material can be deposited on its top surface. The third-layer sheet will continue moving up until all the metal pins have reached their desired positions (Figs. 5e and f).
(5) After the printing process, the third-layer sheet moves down to the original height. During the movement, all the metal pins will be reset to their initial positions (Fig. 5a).
(6) Finally, the metal washers detached from the 3D-printed object are inserted back to the tip of the metal pins. The printing job can then be restarted for the same CAD models; for a printing job with different CAD models, suitable metal tubes can be selected and inserted.

The reusable support height is related to the initial distance between the second-layer and third-layer sheets, the length of the metal tube, and the thickness of the magnetic ring (Fig. 6a). Their relationship can be calculated using Eq. (1).

$$H = L_{Layer2-3} - L_{Tube} - L_{Magnet} \quad (1)$$

The pre-fabricated metal tubes with embedded magnetic rings and magnetic discs are provided to users. They can have standard lengths, such as 5 mm, 10 mm, 15 mm, and so on. Accordingly, users can achieve different heights by inserting the metal tubes with the closest lengths

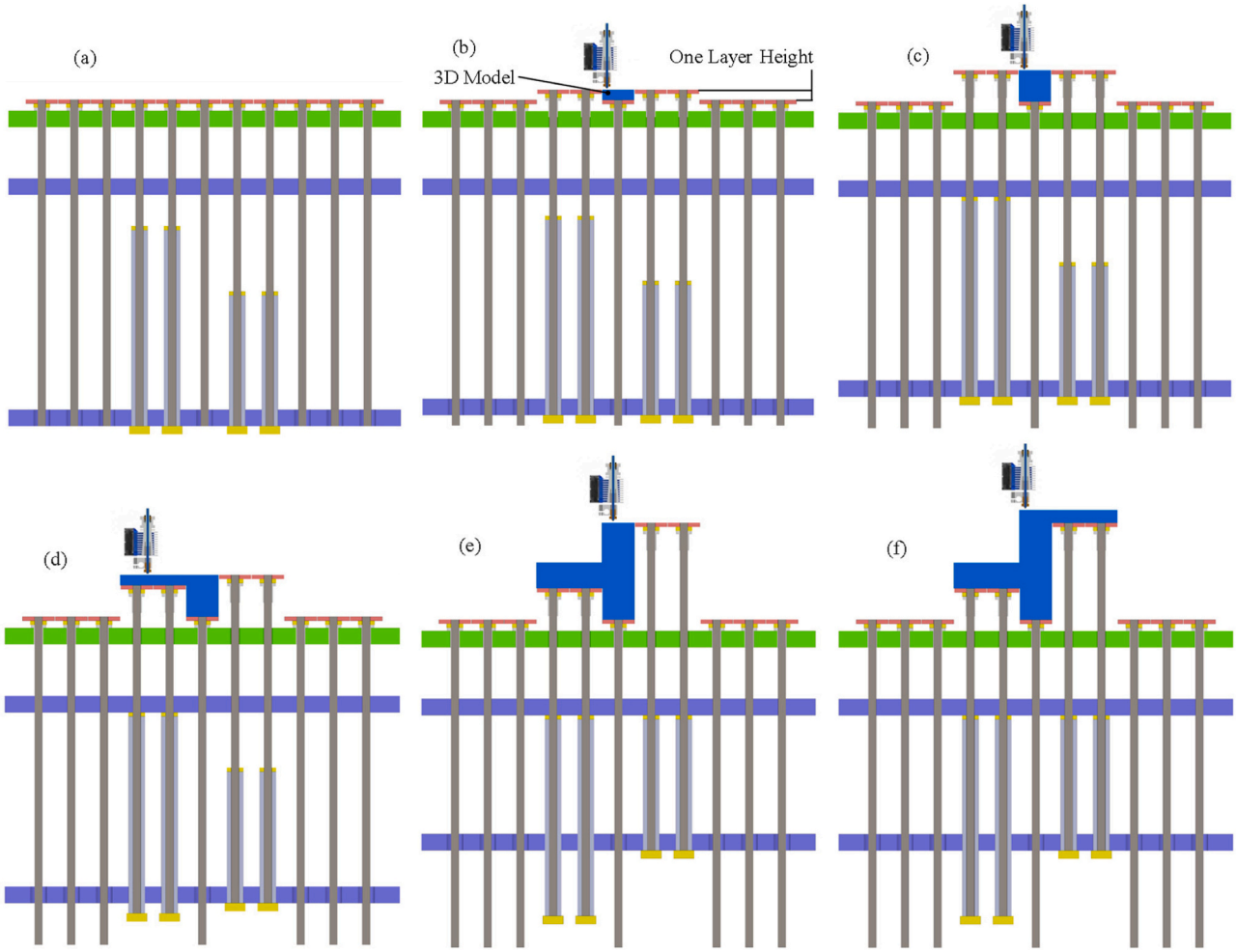

Fig. 5. Sectional view of the FFF process using the reusable support. (a) The original state of the metal pins; (b) the movement of the metal pins after building the first layer; (c, d) the detaching of the metal pins from the moving sheet due to the inserted tubes; and (e, f) the final state of the metal pins.

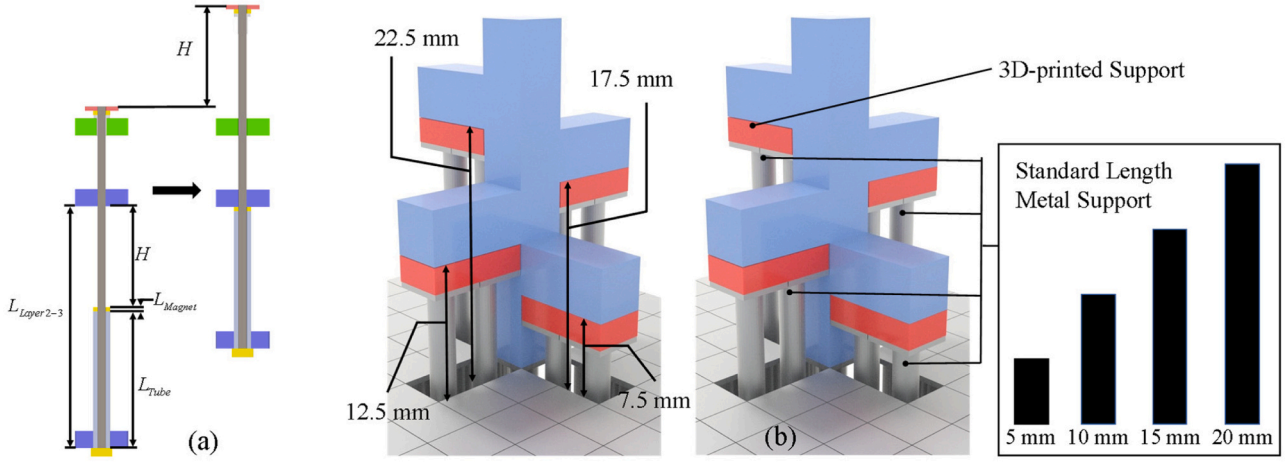

Fig. 6. Achievable heights of the reusable support. (a) The original and final states of a metal pin; and (b) a test case of a CAD model with four overhangs at different heights, and the related metal pins and 3D-printed supports.

from the available tubes. The support structure can be reused for other printing jobs by simply changing metal tubes with different lengths that are inserted onto different pins.

For an arbitrary CAD model, we developed a support generation software system to calculate the position of each metal pin and the related tube length required to achieve its desired height. For a CAD model that requires the support at a height that is different from the provided heights, we will select a smaller tube length that is the closest to the required length based on Eq. (1). The remaining support will be 3D-printed on the top surface of the metal pin. For example, a simple CAD model with four overhangs will be fabricated (Fig. 6b). The heights of the four overhangs are 7.5 mm, 12.5 mm, 17.5 mm, and 22.5 mm, respectively. Suppose the standard heights that the reusable support can achieve are 5 mm, 10 mm, 15 mm, and 20 mm, respectively. Therefore, additional supports with 2.5 mm height will be planned by the software system and 3D-printed on the metal pins.

3. Layout optimization and toolpath planning

3.1. layout optimization problem

For the AM system with the reusable support, a large portion of supports is replaced by metal pins to reduce the printing time and material. The amount of the support that needs to be 3D-printed is affected by three factors: (1) the layout of the CAD model on the printing platform; (2) the height of each metal pin; and (3) the structure of the 3D-printed supports. Many of the aforementioned support structures [24–28] can be directly applied to our research. In this study, we employed the vertical-wall-like structure as the 3D-printed support, since this structure can increase the robustness and reliability of the FFF process.

To achieve the minimum amount of the 3D-printed support, each metal pin should reach its highest level while not intersecting the given CAD model. For the FFF process without the reusable support, the *XY* translation of the model on the printing platform and the rotation of the

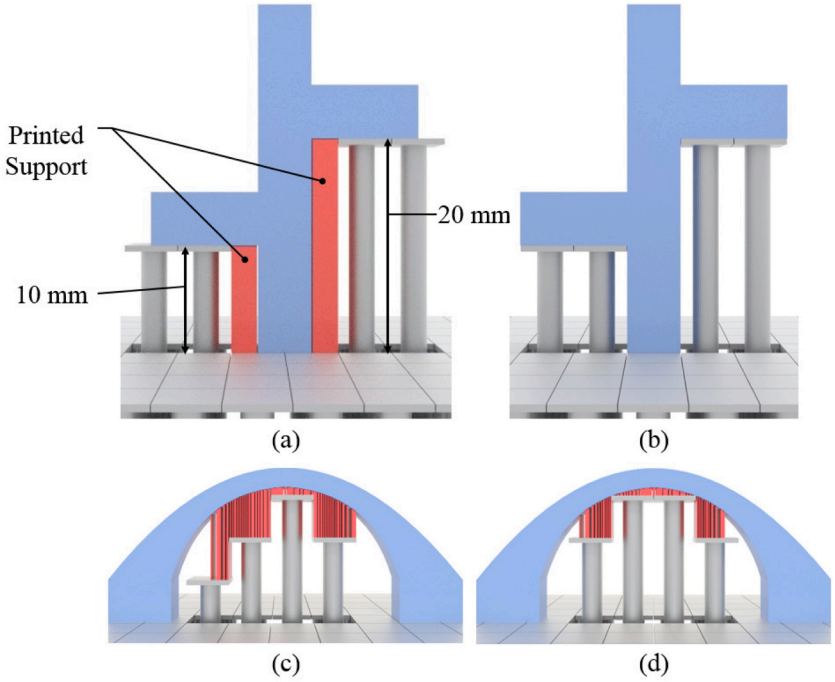

Fig. 7. Comparison of the 3D-printed support between the original layout and the optimized one. The red portions represent 3D-printed support. Each metal pin has a certain *XY* size and achievable Z heights, and cannot intersect the given CAD model. (a) A model before the layout optimization. (b) The same model after the layout optimization. (c) A bridge model before the layout optimization. (d) The bridge model after the layout optimization (For interpretation of the references to color in this figure legend, the reader is referred to the web version of this article).

model around the Z-axis will not change the 3D-printed supports. However, for the FFF process with the reusable support, the layout of an input CAD model on the movable building platform will make a remarkable difference. Two examples are shown in Fig. 7 to illustrate the effect of different layouts. In both test cases, a slight shift of the CAD model on the building platform will make massive differences in the amount of the 3D-printed supports required for the printing job. Therefore, the layout optimization of input CAD models is important to take full advantage of the reusable support.

In this research, suppose a building orientation is given for an input CAD model. We will search the best layout of the CAD model by translating it along the X, Y, and Z axes on the printing platform, and rotate it around the Z-axis (perpendicular to the building platform). Due to the periodic size of the metal pin surface, the translational range in the X and Y directions is $0 \le \Delta x, \Delta y < L$, where L is the surface size of a metal pin. Besides, moving up the part in the Z direction means printing a higher base beneath the model. However, sometimes such Z movement could save more material since a longer metal pin can then be selected from the given standard lengths. The translational range in the Z-axis is $0 \le \Delta z < H_0$, where H_0 is the shortest standard length given in the metal tubes (e.g., 5 mm in our study). The rotational range of the model around the Z-axis is $0 \le \theta_Z < 2\pi$.

3.2. Layout optimization formulation

For a given CAD model with a rotation angle $\theta_Z$around the Z-axis, suppose the projection of the region to add supports on the printing platform is represented by $S_{XY\theta_Z}$. The support height of each point within $S_{XY\theta_Z}$ is $z(x,y)$. Then the maximal 3D-printed support volume is:

$$V_0 = \iint_{S_{XY\theta_Z}} z(x,y)ds \tag{2}$$

Suppose the movable printing platform is composed of $m \times n$ metal pins, where m is the number of rows and n is the number of columns. The range of each metal pin is $P_{r,s}$, and its corresponding height is $H_{r,s}$. Then the whole printing platform can be expressed as a set:

$$P = \{P_{r,s} | 0 \le r < m, 0 \le s < n\} \tag{3}$$

Hence the total material cost for the 3D-printed support $C_{material}(\Delta x, \Delta y, \Delta z, \theta_Z)$ after employing the reusable support is:

$$C_{material} = V_0 - \sum_{P_{r,s} \in P} |P_{r,s} \cap S_{XY\theta_Z}| H_{r,s} \tag{4}$$

To fulfill the potential of the reusable support, the height of each metal pin should be:

$$H_{r,s} = \min_{(x,y) \in P_{r,s}} H_0 \lfloor z(x,y)/H_0 \rfloor \tag{5}$$

The number of metal pins to be used is desired to be less to cut down the setup time. The number of the used metal pins is:

$$C_{pin} = \sum_{H_{r,s}>0} 1 \tag{6}$$

Also, printing at the center of each metal pin surface is more reliable than printing at the boundary of the metal pin surface (Fig. 4a). We can also incorporate such hardware constraint in the layout optimization. Suppose $E_{r,s} \subset P_{r,s}$ is the edge of each pin. Then the total area of the 3D-printed supports located at the boundary region of the metal pins is:

$$C_{edge} = \sum_{H_{r,s}>0} |E_{r,s} \cap S_{XY\theta_Z}| \tag{7}$$

Therefore, the objective function for the layout optimization problem based on the reusable support is formulated as:

$$\begin{aligned} \min C(\Delta x, \Delta y, \Delta z, \Delta\theta) &= \min_{\Delta x, \Delta y, \Delta z, \Delta\theta} \left(C_{material} + \alpha C_{pin} + \beta C_{edge} \right) \\ &= \min_{\Delta x, \Delta y, \Delta z, \Delta\theta} \left(V_0 - \sum_{P_{r,s} \in P} |P_{r,s} \cap S_{XY\theta_Z}| H_{r,s} + \alpha \sum_{H_{r,s}>0} 1 + \beta \sum_{H_{r,s}>0} |E_{r,s} \cap S_{XY\theta_Z}| \right) \end{aligned} \tag{8}$$

subject to: $0 \le \Delta x, \Delta y < L; 0 \le \Delta z < H_0; 0 \le \theta_Z < 2\pi$.

3.3. Computation strategy based on discretization and enumeration

Fig. 8 shows a simple door model to illustrate the challenges in solving the layout optimization problem. Although all the design variables (Δx, Δy, Δz, and θ_Z) are continuous, the required 3D-printed support for a given layout is a step function to avoid the collision of the reusable support with the CAD model. In this test case, the required 3D-printed support only has two values (Figs. 8b and c) due to the discontinuity of the metal pins and their limited surface sizes and heights. For such a discrete optimization problem, it is challenging to adopt a conventional iterative optimization method. In comparison, the enumeration method can guarantee a good search result and lead to a more robust result. In this paper, we develop an effective and efficient enumeration method to compute the layout solution that can satisfy the requirements of the reusable support.

Our computational procedure based on the enumeration method is given as follows. First, a 3D CAD model is sliced into a set of two-dimensional (2D) polygons, which indicates the shape of each 2D layer. The layout optimization begins based on the sliced 2D layers. Note V_0 in the objective function (8) is always a constant if the model is not moved along the Z-axis. Regarding the other three items in Eq. (8), computing $H_{r,s}$ costs most of the running time in each iteration. To accelerate the search process, we approximate the variables by discretizing the printing platform. That is, the movable building platform defined by each metal pin is further divided into K^2 grids ($K = 50$ was used in our study). Each grid is a sampling point that records the shortest distance between the printing platform and the CAD model (Fig. 9).

This process can be viewed as shooting a ray from each sampling point and intersect with the sliced polygons of the CAD model [35,36]. Only the lowest layer number with the intersection will be recorded. The grids that do not intersect with the CAD model are marked by $+\infty$. Hence the whole printing platform can be represented by a $mK \times nK$ matrix h, which is called the heightmap of an input CAD model:

$$h = \{h_{i,j} | 0 \le i < m \times K, 0 \le j < n \times K\} \tag{9}$$

The minimum layer serial number within each metal pin range $P_{r,s}$ determines the maximum height of each metal pin $H_{r,s}$. This is a classical 2D Range Minimum Query (RMQ) problem and can be processed quite fast using dynamic programming. The pre-processing stage takes

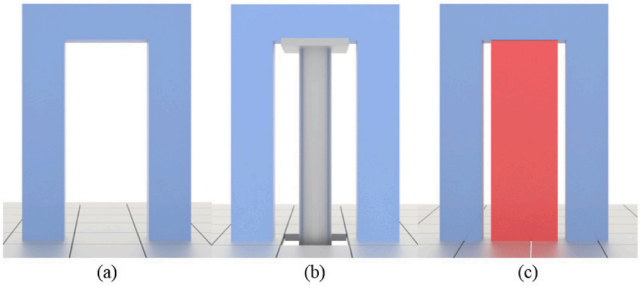

Fig. 8. Illustration of the discontinuity in the 3D-printed support volume during the layout optimization. (a) Original door model without any support. (b) A layout requires no 3D-printed support. (c) A layout requires the maximal 3D-printed support. Note the CAD model is just slightly moved in the X-axis from its position in (b).

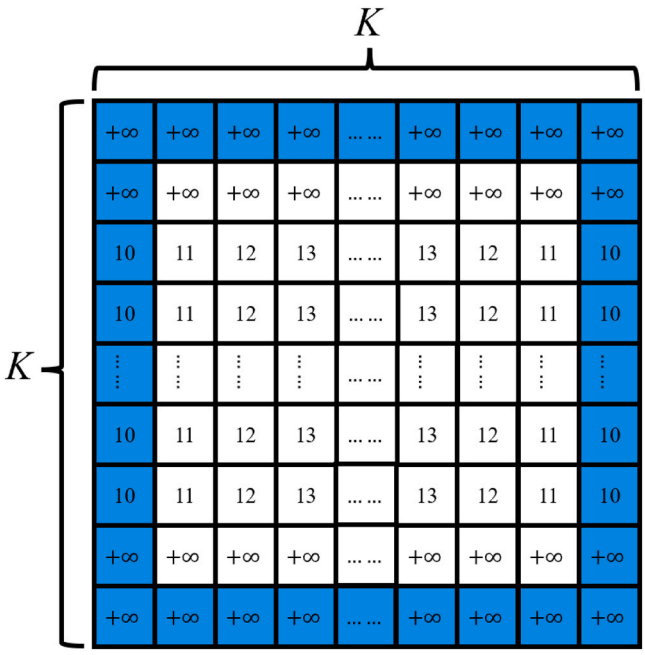

Fig. 9. Discretization of the movable platform of a metal pin with its boundary region highlighted in blue (For interpretation of the references to color in this figure legend, the reader is referred to the web version of this article).

$O(K^2(\lg K)^2)$ time, and the query stage only takes $O(1)$ time.

After digitizing the printing platform, the material consumption to print support $C_{material}$ is converted into the sum of the height at each sampling point that intersects the CAD model:

$$C_{material} = \sum_{P_{r,s}\in P} \sum_{(i,j)\in P_{r,s}} (h_{i,j} - H_{r,s}) \tag{10}$$

Similarly, the total area of the 3D printed support located at the boundary region of the lifted metal pins (see the blue regions in Fig. 9) can be computed by the number of the grids:

$$C_{edge} = \sum_{\substack{H_{r,s}>0 \\ h_{i,j}\neq+\infty,(i,j)\in E_{r,s}}} 1 \tag{11}$$

At this point, the value of the objective function can be calculated. Note the heightmap will change in each iteration due to the XY translation and the Z rotation of the CAD model. The step size of Δx and Δy in the search is L/K. The step size θ_z is $2\pi/N$ (e.g., $N = 360$ was used in our test cases). Instead of transforming the model, the heightmap can be updated quickly by translating the initial height map directly. Moreover, the translation of the heightmap matrix can be achieved by re-querying the elements of different indexes. However, after each rotation around the Z-axis, the heightmap needs to be recomputed before querying. Therefore, the total time complexity is $O(K^2N(\lg K)^2)$. The computation in the layout optimization is largely dependent on the step size used in the search, while the number of the triangles of the CAD model has little effect on the computation time.

As to the translation in the Z direction, we only check and compare the value of the objective function in the final step. That is, the translational distance must be the multiples of the layer thickness that is smaller than the minimum length of the provided metal tubes. Therefore, we only need to increase the minimum layer number of each metal pin by the multiples within the Z translational range and recalculate the height of each metal pin $H_{r,s}$. After these operations, the optimized layout of the part on the building platform is identified.

3.4. Toolpath of 3D-printed support on metal pins

The amount of reusable support has been determined after the layout optimization of given CAD models. Based on the planned reusable support, the strategy of printing additional supports on the lifted metal pins needs to be considered. Note each metal pin is at different heights, and the top surface of a metal pin is relatively small (12.7 mm × 12.7 mm in our setup). Hence, how to efficiently deposit material on such a small area without constantly turning on and off the extruding nozzle is a critical problem to be addressed. Zhao et al. [37] developed a new kind of "space-filling" pattern called connected Fermat spirals. This pattern can fill an arbitrary 2D polygon without a large change of curvature. The spiral can also start and end in any given points on the polygon, which provides more freedom in determining the path between different metal pins. In addition, this type of pattern is more stable than the traditional infill patterns, such as zigzag and grid. In this research, we used connected Fermat spirals as the toolpath of the 3D-printed support on a metal pin's surface.

In the layout optimization discussed in Section 3.3, a heightmap h defined as a $mK \times nK$ matrix has been generated for a CAD model to compute an optimized layout. Accordingly, we construct the tool path of the 3D-printed support based on the sampling grids marked by the layer serial numbers in the heightmap h. Within each metal pin, the marked grids are connected into a set of convex polygons (Fig. 10a–c). To fill each polygon with connected Fermat spirals, the level set of each polygon (defined as the distance to the boundary) is computed by shrinking the convex polygons equidistantly (Fig. 10d). By connecting the neighboring polygons to fill each convex polygon, the sample grids are converted into connected Fermat spirals, and the generated toolpath can be converted into the G-code for the FFF process (Fig. 10e).

The entry point and the exit point of each polygon can be specified before cutting and re-linking the level set of each polygon. Also, the printing order of the polygons needs to be determined to reduce the travel distance. In our study, we simply calculate the center of each polygon (x_i, y_i) and sort them based on the sums of x_i and y_i. Suppose the origin is at the top left corner of the printing platform. The printing process will always start from the top left corner to the bottom right corner for one layer and reverses the order for the next layer. Then the entry and exit points of the outermost polygon can be determined by the minimum distance between two neighboring level sets according to the specified printing order.

Suppose the entry point and the exit point of an outermost polygon are represented by S_0 and E_0, respectively (Fig. 11a). Accordingly, the entry points and exit points of the inner polygons of the level set can be determined by the closest points on the next inner polygon from the outer one. Therefore, the following entry point $S_1$and exit point E_1 that are the nearest points to S_0 and E_0 can be found on the neighboring inner polygon. Repeat the process, and we will have a set of points $S_0, S_1, S_2, \cdots$ and $E_0, E_1, E_2, \cdots$ (Fig. 11b). For each S_i and E_i (excluding the innermost ones), we set a point ε mm away anti-clockwise on the same polygon as S_i^p and E_i^p. Then we cut each polygon except the innermost one into two portions f_i^+, f_i^- by deleting the segments $S_iS_i^p$ and $E_iE_i^p$ (Figs. 11b and c). For the innermost polygon, we only keep the shortest segment. Finally, Figs. 11d and e show the separated curves. Accordingly, $f_0^+, f_1^-, f_2^+, \cdots$ form the clockwise portion of the connected Fermat spiral and $f_0^-, f_1^+, f_2^-, \cdots$ form the anti-clockwise portion of the spiral. Finally, one continuous Fermat spiral can be connected and saved as the G-code for the FFF process..

4. Validation and analysis

4.1. A prototype system based on FFF

A prototype FFF system that incorporates the reusable support has been built to test the presented design and the related building process

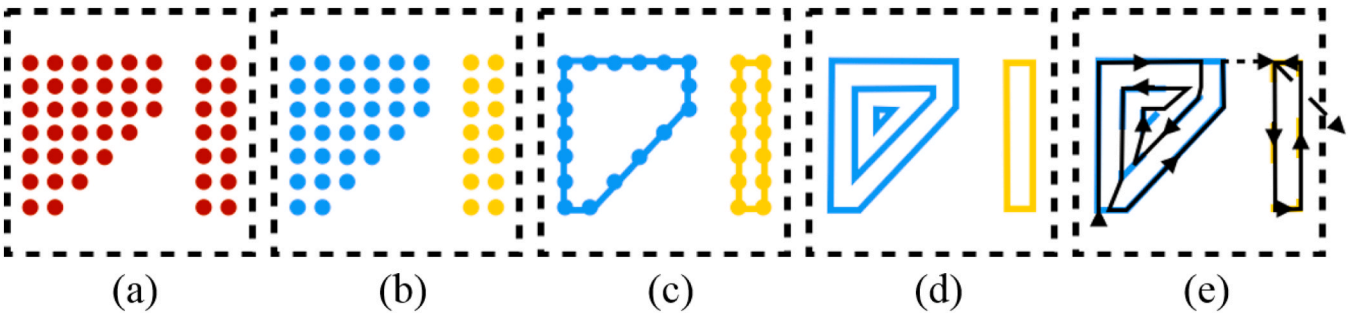

Fig. 10. Constructing Fermat spirals within a pin. (a) Supporting grids allocated to a pin. (b) Grouping of neighboring grids. (c) A convex polygon is constructed for each group of grids. (d) Level set of the boundary polygons. (e) The connected Fermat spirals as the toolpath for the FFF process.

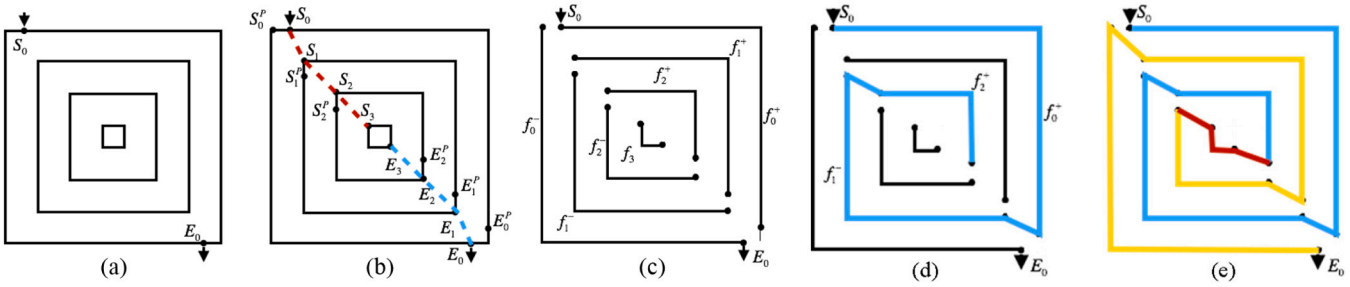

Fig. 11. Partition of a level set and the connection of the segmented curves. (a) The entry point and the exit point of the outermost polygon. (b) Entry points and exit points of the inner polygons. (c) Segmented curves are based on the entry and exit points. (d) The clockwise portion of the Fermat spiral. (e) The connected Fermat spiral as the toolpath for the printing process.

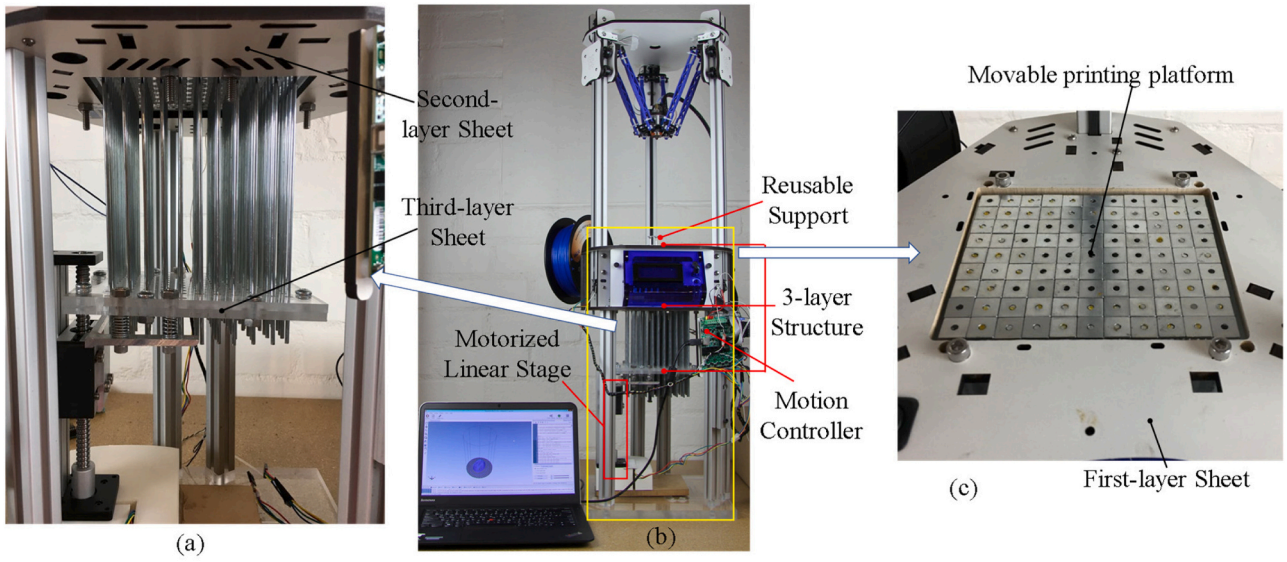

Fig. 12. A prototype system with reusable support. (a) The second-layer and third-layer sheets of the reusable support. (b) A revised FFF 3D printer with reusable support. (c) The building platform is defined by 11 × 9 metal pins (For interpretation of the references to color in this figure legend, the reader is referred to the web version of this article).

(Fig. 12). The prototype system was constructed based on a low-cost commercial FFF 3D printer (Orion Delta). The reusable support was added to the bottom of the 3D printer and highlighted in the yellow box (Fig. 12b). The printing platform was composed of 9 × 11 metal pins (Fig. 12c). The size of the washer on the top of each metal pin is 12.7 mm × 12.7 mm. If smaller washers are used, more metal pins could be used to serve as the programmable building platform, which leads to more savings on printing time and material. The first-layer sheet is a fixed acrylic sheet that supports the metal pins. The square washers sitting on the acrylic sheet were purchased off-the-shelf (from McMaster-Carr). They are flat with thickness variance less than 0.08 mm. Therefore, the printing platform is flat with controlled height variation, which is satisfactory for the FFF process. The second-layer and third-layer sheets are also made of acrylic to save cost (Fig. 12a). We embedded some metal washers in the acrylic sheets around the drilled holes to achieve the magnetic effect required by the metal pin structure (Fig. 3).

4.2. Layout optimization and control software

The presented layout optimization and toolpath generation methods were implemented using Visual C++ and integrated with an open-source FFF slicer (Slic3r). In the development, we also used a library libigl [38] for mesh processing. The graphical user interface of the developed software system is shown in Fig. 13.

As mentioned before, an additional motorized linear stage is used to push up the metal pins (Fig. 3). We defined its motion as A-axis in the G-code. Accordingly, a command "G1 Axxx" was added between the G-code of two adjacent layers to control the movement of the metal pins, where "xxx" is the travel distance. Compared with the normal FFF process, the reusable support moves after the fabrication of each layer. Accordingly, the G-code exported from our slicing software was loaded into the client software (Repetier-Host 1.6.2) to communicate with the modified Repetier firmware 0.91. When the motion controller executes our self-defined command, the linear stage will lift the metal pins with inserted metal tubes by one-layer distance.

The developed software system was tested using the planned physical experiments. All the test cases were performed on a personal computer equipped with Intel Core i7 6770 3.4 GHz and 8 GB memory. We measured the execution time of the layout optimization and the entire computation process from the input of an STL file to the output of the G-code. Table 1 shows the collected running time. The layout optimization discussed in Section 3 took most of the computation time. The computational performance based on the enumeration method is satisfactory. In general, the total running time of all the test cases is within 30 s.

4.3. Experimental results

A comparison of the fabrication results with and without the reusable support is shown in Fig. 14. After generating the planned layout and the required toolpath, we used commercially available acrylonitrile butadiene styrene (ABS) and polylactic acid (PLA) filaments to build the test parts (ABS for Fig. 14a, and PLA for Figs. 1 and 14c, e, h). The printing speed was set at 30 mm/s. The layer thickness was set to 0.2 mm, which is commonly used in commercial FFF 3D printers. For a layer thickness that is not a divisor of the standard reusable support height, 3D printed supports with variant thickness can be deposited on the lifted printing platform using toolpath planning techniques such as a faster moving speed or a slower feeding rate. Two groups of the tests, with and without the reusable supports, were fabricated so the experimental results can be compared side by side. The same building parameters were used in building the two groups of tests. The same toolpath for the CAD model and the internal support was used in all the tests.

Table 1
Running time statistics of the software system.

Printing examples	Figure index	Running time of layout optimization	Total running time
Gymnast	Fig. 1	27.6 s	28.0 s
Four-overhang	Fig. 14a	26.2 s	26.5 s
Bridge	Fig. 14c	25.6 s	25.8 s
Teapot	Fig. 14e	26.3 s	26.8 s
Helmet	Fig. 14h	31.4 s	34.0 s

In our prototype system, the standard lengths of the reusable support were the multiples of 5 mm. Since the heights of the four overhangs for the model (Fig. 14a) are 15 mm, 30 mm, 45 mm, and 60 mm, respectively, no additional support is needed. For all the other test models, additional 3D-printed support was required; however, the 3D-printed support was much less due to the added reusable support. In addition to reducing printing time and material waste, the 3D-printed support that is significantly shortened enhances the reliability of the printing process, since the torque added by the moving nozzle has less effect on the metal pin. For example, Fig. 1b shows a long pillar required for the right foot of the gymnast (highlighted inside a solid box). The support was gradually bent in the printing process, which may cause the printing failure. In contrast, the 3D-printed support based on the movable metal pins was much shorter (Fig. 1a).

Note no changes are made for the supports that do not touch the building platform. For example, some internal supports are required inside the handle of the teapot (Figs. 14e and f). For both tests with and without reusable support, the same 3D-printed support was used. However, for the internal supports that can be reached from the building

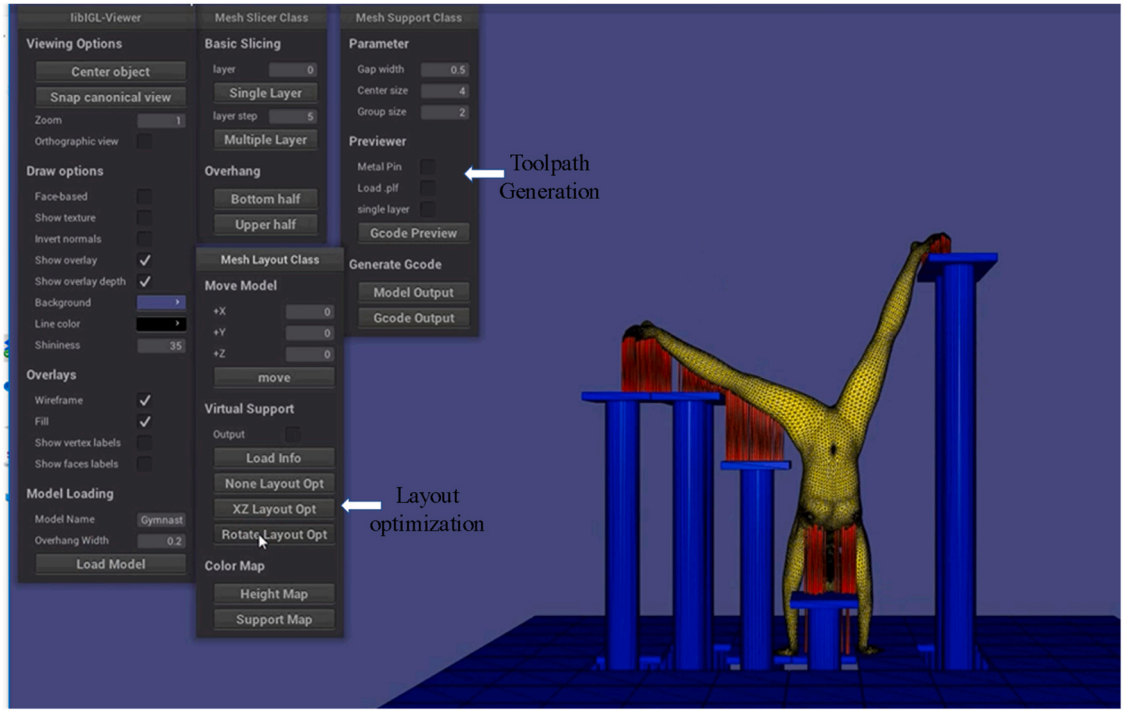

Fig. 13. The graphical user interface (GUI) of the software system developed for the FFF 3D printer with reusable metal support.

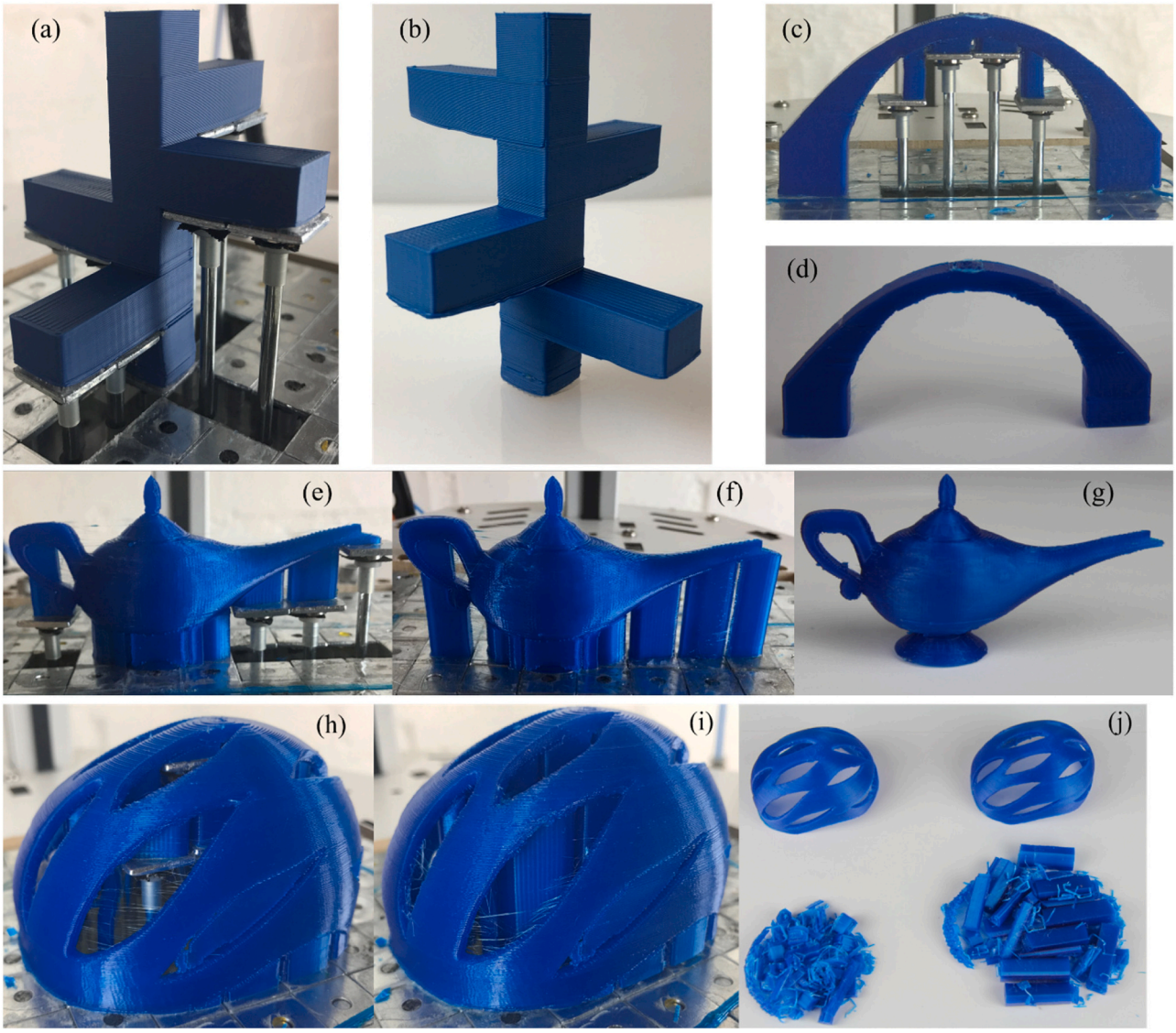

Fig. 14. Printing results of the test cases. (a) The printing result of a four-overhang model with reusable support; (b) the 3D-printed part after the cleanup; (c) the printing result of a bridge model with reusable support; (d) the printed bridge after the cleanup; (e) the printing result of a teapot model with reusable support; (f) the printing result of the teapot without reusable support; (g) the printed teapot after the cleanup; (h) the printing result of a helmet model with reusable support; (i) the printing result of the helmet without reusable support; and (j) a comparison of the supporting material in (h) and (i).

Table 2
Statistics of the printing test cases.

Printing examples	Printing time without reusable support	Printing time with reusable support	Material consumption without reusable support	Material consumption with reusable support	Time saving in printing whole part	Material saving in printing whole part	Time saving in printing support	Material saving in printing support
Gymnast (Fig. 1)	380 min	173 min	3936 mm	2152 mm	54.5%	45.3%	76.1%	78.1%
Four-overhang (Fig. 14a)	440 min	157 min	18,420 mm	7540 mm	64.3%	59.1%	100%	100%
Bridge (Fig. 14c)	207 min	142 min	8313 mm	5461 mm	31.4%	34.3%	70.7%	75.7%
Teapot (Fig. 14e)	262 min	225 min	5401 mm	4646 mm	14.1%	14.0%	20.9%	22.6%
Helmet (Fig. 14h)	921 min	568 min	20,629 mm	12,543 mm	38.3%	39.2%	52.6%	62.2%
Average					**38.1%**	**35.3%**	**63.0%**	**64.7%**

platform, reusable support will be used. For example, nine metal pins were used to provide a raised building platform inside the helmet (Fig. 14h). Hence much less 3D-printed support is needed in the printing job. Fig. 14j shows a comparison of the collected supporting material after the fabrication process. Future enhancements of the prototype include adding an enclosed printing chamber with a heating element to maintain a constant chamber temperature during the printing process. Better temperature control can prevent ABS from warping on the reusable support surface (Fig. 14a). For other test cases using PLA (Figs. 1 and 14c, e, h), no warpage occurred on the current prototype.

Table 2 summarizes the printing statistics of all the test cases, including printing time, material consumption (support only), and the percentage of the reduction in printing time and material consumption (both part and support). The statistics show that reusable support brings a significant reduction in both printing time and material waste. The average saving on the supporting material is 64.7% (ranging from 22.6% to 100%) compared with the traditional printing process. The average saving on the printing time is 63.0% (ranging from 20.9% to 100%) if considering only the support, and 38.1% (ranging from 14.1% to 64.3%) if considering the printing job. Our study has also demonstrated the improvement in printing reliability for the FFF process. How to apply the reusable support principle to other AM processes is an open question that needs to be further investigated by the AM research community.

5. Conclusion and future work

We present a novel support generation strategy and a reusable support design for additive manufacturing. The new reusable support method has been demonstrated using the fused filament fabrication process. In our design, a single motor is used to drive a large number of metal pins serving as a programmable building platform to different Z heights. Consequently, after stopping at a pre-defined height, each metal pin can provide a printing surface to deposit printing materials. After the printing process finishes, the metal pins can be reset for the next printing job. In addition to the hardware design, we present critical software challenges for the reusable support, including the layout optimization of input CAD models and the toolpath generation on the small pin surface. We introduce an efficient computation algorithm based on discretization and enumeration and a toolpath generation method based on connected Fermat spirals to address the challenges. Several test cases have been presented to demonstrate the effectiveness of the reusable support method. In addition to the reduction of printing time and material waste, the fabrication process using the reusable support is more reliable and robust, especially for parts with tall overhang features.

In the future, we would like to investigate the reusable support for the FFF process with a larger area. A critical challenge for the big area additive manufacturing (BAAM) is the long printing time. The reusable support may provide a feasible solution to significantly reduce the printing time of BAAM. For the material extrusion processes such as direct ink writing (DIW), the printing materials, especially those used in the bio-related study, could be expensive. We will reduce the metal pin size for such processes to further increase the material saving. Finally, we will investigate the extension of the reusable support method to other AM processes such as the projection-based stereolithography and the powder-based selective laser melting. In addition to their unique issues like separation issue [39], such AM processes are all facing the common support generation challenges, i.e., sufficient support needs to be added for the printing process, and, at the same time, the added support needs to be easily removed after the printing process. The reusable support could provide a new direction to address such a dilemma in support generation in the future.

CRediT authorship contribution statement

Yang Xu: Writing - original draft, Hardware, Software, Analysis, Visualization, Data analysis. **Ziqi Wang:** Writing - original draft, Software. **Siyu Gong:** Hardware, Data analysis. **Yong Chen:** Conceptualization, Methodology, Resources, Supervision, Writing - review & editing.

Declaration of Competing Interest

The authors declare that they have no know competing financial interests or personal relationships that could have appeared to influence the work reported in this paper.

Acknowledgments

The authors acknowledge the fellowship support and the visiting scholar program from Viterbi School of Engineering at the University of Southern California.

References

[1] W. Gao, Y. Zhang, D. Ramanujan, K. Ramani, Y. Chen, C.B. Williams, C.C.L. Wang, Y.C. Shin, S. Zhang, P.D. Zavattieri, The status, challenges, and future of additive manufacturing in engineering, Comput. Des. 69 (2015) 65–89, https://doi.org/10.1016/j.cad.2015.04.001.
[2] G.J. Artz, J.L. Lombardi, D. Popovich, Water soluble rapid prototyping support and mold material, 2010.
[3] J. Jin, Y. Chen, Highly removable water support for stereolithography, J. Manuf. Process. 28 (2017) 541–549, https://doi.org/10.1016/j.jmapro.2017.04.023.
[4] J. Jiang, X. Xu, J. Stringer, Support structures for additive manufacturing: a review, J. Manuf. Mater. Process. 2 (2018) 64, https://doi.org/10.3390/jmmp2040064.
[5] B. Ezair, F. Massarwi, G. Elber, Orientation analysis of 3D objects toward minimal support volume in 3D-printing, Comput. Graph. 51 (2015) 117–124, https://doi.org/10.1016/j.cag.2015.05.009.
[6] W. Cheng, J.Y.H. Fuh, A.Y.C. Nee, Y.S. Wong, H.T. Loh, T. Miyazawa, Multi-objective optimization of part- building orientation in stereolithography, Rapid Prototyp. J. 1 (1995) 12–23, https://doi.org/10.1108/13552549510104429.
[7] D. Frank, G. Fadel, Expert system-based selection of the preferred direction of build for rapid prototyping processes, J. Intell. Manuf. 6 (1995) 339–345, https://doi.org/10.1007/BF00124677.
[8] P. Alexander, S. Allen, D. Dutta, Part orientation and build cost determination in layered manufacturing, Comput. Des. 30 (1998) 343–356, https://doi.org/10.1016/S0010-4485(97)00083-3.
[9] J. Majhi, R. Janardan, M. Smid, P. Gupta, On some geometric optimization problems in layered manufacturing, Comput. Geom. 12 (1999) 219–239, https://doi.org/10.1016/S0925-7721(99)00002-4.
[10] P.M. Pandey, K. Thrimurthulu, N.V. Reddy *, Optimal part deposition orientation in FDM by using a multicriteria genetic algorithm, Int. J. Prod. Res. 42 (2004) 4069–4089, https://doi.org/10.1080/00207540410001708470.
[11] R. Paul, S. Anand, Optimization of layered manufacturing process for reducing form errors with minimal support structures, J. Manuf. Syst. 36 (2015) 231–243, https://doi.org/10.1016/j.jmsy.2014.06.014.
[12] P. Das, R. Chandran, R. Samant, S. Anand, Optimum part build orientation in additive manufacturing for minimizing part errors and support structures, Procedia Manuf. 1 (2015) 343–354, https://doi.org/10.1016/j.promfg.2015.09.041.
[13] A.M. Mirzendehdel, K. Suresh, Support structure constrained topology optimization for additive manufacturing, Comput. Des. 81 (2016) 1–13, https://doi.org/10.1016/j.cad.2016.08.006.
[14] M. Yao, Z. Chen, L. Luo, R. Wang, H. Wang, Level-set-based partitioning and packing optimization of a printable model, ACM Trans. Graph. 34 (2015) 1–11, https://doi.org/10.1145/2816795.2818064.
[15] J. Vanek, J.A.G. Galicia, B. Benes, R. Měch, N. Carr, O. Stava, G.S. Miller, PackMerger: a 3D print volume optimizer, Comput. Graph. Forum 33 (2014) 322–332, https://doi.org/10.1111/cgf.12353.
[16] R. Hu, H. Li, H. Zhang, D. Cohen-Or, Approximate pyramidal shape decomposition, ACM Trans. Graph. 33 (2014) 1–12, https://doi.org/10.1145/2661229.2661244.
[17] J. Jiang, X. Xu, J. Stringer, Optimisation of multi-part production in additive manufacturing for reducing support waste, Virtual Phys. Prototyp. 14 (2019) 219–228, https://doi.org/10.1080/17452759.2019.1585555.
[18] Y. Chen, K. Li, X. Qian, Direct geometry processing for telefabrication, J. Comput. Inf. Sci. Eng. 13 (2013) 1–15, https://doi.org/10.1115/1.4024912.
[19] Y.-S. Leung, T.-H. Kwok, X. Li, Y. Yang, C.C.L. Wang, Y. Chen, Challenges and status on design and computation for emerging additive manufacturing technologies, J. Comput. Inf. Sci. Eng. 19 (2019) 1–21, https://doi.org/10.1115/1.4041913.
[20] X. Huang, C. Ye, S. Wu, K. Guo, J. Mo, Sloping wall structure support generation for fused deposition modeling, Int. J. Adv. Manuf. Technol. 42 (2009) 1074–1081, https://doi.org/10.1007/s00170-008-1675-2.
[21] G. Strano, L. Hao, R.M. Everson, K.E. Evans, A new approach to the design and optimisation of support structures in additive manufacturing, Int. J. Adv. Manuf. Technol. 66 (2013) 1247–1254, https://doi.org/10.1007/s00170-012-4403-x.
[22] S. Cacace, E. Cristiani, L. Rocchi, A level set based method for fixing overhangs in 3D printing, Appl. Math. Model. 44 (2017) 446–455, https://doi.org/10.1016/j.apm.2017.02.004.

[23] R. Schmidt, N. Umetani, Branching support structures for 3D printing. ACM SIGGRAPH, ACM Press, New York, New York, USA, 2014, https://doi.org/10.1145/2619195.2656293.
[24] J. Vanek, J.A.G. Galicia, B. Benes, Clever support: efficient support structure generation for digital fabrication, Comput. Graph. Forum 33 (2014) 117–125, https://doi.org/10.1111/cgf.12437.
[25] J. Dumas, J. Hergel, S. Lefebvre, Bridging the gap: automated steady scaffoldings for 3D printing, ACM Trans. Graph. 33 (2014) 1–10, https://doi.org/10.1145/2601097.2601153.
[26] J. Jiang, J. Stringer, X. Xu, R.Y. Zhong, Investigation of printable threshold overhang angle in extrusion-based additive manufacturing for reducing support waste, Int. J. Comput. Integr. Manuf. 31 (2018) 961–969, https://doi.org/10.1080/0951192X.2018.1466398.
[27] J. Jiang, J. Stringer, X. Xu, Support optimization for flat features via path planning in additive manufacturing, 3D Print. Addit. Manuf. 6 (2019) 171–179, https://doi.org/10.1089/3dp.2017.0124.
[28] J. Jiang, X. Xu, J. Stringer, Optimization of process planning for reducing material waste in extrusion based additive manufacturing, Robot. Comput. Integr. Manuf. 59 (2019) 317–325, https://doi.org/10.1016/j.rcim.2019.05.007.
[29] E. Barnett, C. Gosselin, Weak support material techniques for alternative additive manufacturing materials, Addit. Manuf. 8 (2015) 95–104, https://doi.org/10.1016/j.addma.2015.06.002.
[30] S. Hongyao, Y. Xiaoxiang, F. Jianzhong, Research on the flexible support platform for fused deposition modeling, Int. J. Adv. Manuf. Technol. 97 (2018) 3205–3221, https://doi.org/10.1007/s00170-018-2046-2.
[31] H. Zhu, W.J. Book, Control concepts for digital clay, IFAC Proc. Vol. 36 (2003) 347–352, https://doi.org/10.1016/S1474-6670(17)33418-3.
[32] H. Zhu, W.J. Book, Practical structure design and control for digital clay, in: Dynamic Systems and Control Parts A B, ASMEDC, 2004, pp. 1051–1058. doi: 10.1115/IMECE2004-59743.
[33] D. Leithinger, S. Follmer, A. Olwal, H. Ishii, Shape displays: spatial interaction with dynamic physical form, IEEE Comput. Graph. Appl. 35 (2015) 5–11, https://doi.org/10.1109/MCG.2015.111.
[34] H. Ishii, D. Leithinger, S. Follmer, A. Zoran, P. Schoessler, J. Counts, TRANSFORM. Proceedings of the 33rd Annual ACM Conference Extended Abstracts on Human Factors in Computing Systems – CHI EA '15, ACM Press, New York, New York, USA, 2015, pp. 687–694, https://doi.org/10.1145/2702613.2702969.
[35] C.C.L. Wang, Y.-S. Leung, Y. Chen, Solid modeling of polyhedral objects by layered depth-normal images on the GPU, Comput. Des. 42 (2010) 535–544, https://doi.org/10.1016/j.cad.2010.02.001.
[36] Y. Chen, C.C.L. Wang, Regulating complex geometries using layered depth-normal images for rapid prototyping and manufacturing, Rapid Prototyp. J. 19 (2013) 253–268, https://doi.org/10.1108/13552541311323263.
[37] H. Zhao, F. Gu, Q.-X. Huang, J. Garcia, Y. Chen, C. Tu, B. Benes, H. Zhang, D. Cohen-Or, B. Chen, Connected fermat spirals for layered fabrication, ACM Trans. Graph. 35 (2016) 1–10, https://doi.org/10.1145/2897824.2925958.
[38] A. Jacobson, D. Panozzo, libigl – A simple C++ geometry processing library, 2014. http://libigl.github.io/libigl/ (Accessed February 2017).
[39] Y. Xu, Y. Zhu, Y. Sun, J. Jin, Y. Chen, A vibration-assisted separation method for constrained-surface-based stereolithography, J. Manuf. Sci. Eng. 143 (2021) 1–29, https://doi.org/10.1115/1.4048445.